A Prony-Based Curve-Fitting Method for Characterization of RF Pulses From Optoelectronic Devices

Saptarshi Mukherjee, Karen Dowling, Yicong Dong, Kexin Li, *Graduate Student Member, IEEE*, Adam Conway, *Member, IEEE*, Shaloo Rakheja, *Member, IEEE*, and Lars Voss

***Abstract*—There has been a boost in optoelectronic device technology that can leverage strengths of both optical and electronic worlds to support high-voltage and high-speed operation. It is critical to characterize the RF performance from the measured signals of these devices in order to evaluate their performance, optimize their designs and also aid in better understanding of the device physics. Conventional curve-fitting models either fail to fit measured signals with high accuracy or provide limited, if any, information about the device physics. Here, we propose a Prony-based curve-fitting method to characterize RF pulse measurements from such optoelectronic devices. The performance of the overall algorithm on measurement data shows high accuracy, with the capability to extract key pulse parameters such as full width at half maximum and rise time. Additionally, the capability of the method to extract time constants associated with semiconductor traps can help in better understanding of optoelectronic device physics.**

***Index Terms*—Curve fitting, Gaussian distribution, optoelectronic devices, Prony method, RF signals, signal analysis.**

I. Introduction

THERE has been a boost in optoelectronic devices that combine the strengths of both optical and electronic worlds: specifically the speed of light with the power handling capability of wide bandgap semiconductor materials [1]–[3]. This technology will be capable of operating at 100 s of GHz with bandwidths of 10 s of GHz, output power in the 100 s of watts within a compact form factor [4]. Thus, it will be relevant for various applications such as wireless communication, cyber security, radar, electronic warfare, remote sensing and non-destructive characterization using Terahertz radiation [5]–[8].

Curve-fitting techniques are required to characterize the performance of the optoelectronic devices from the measured signals to optimize their designs and also aid in better understanding of the semiconductor device physics from the measured signals of these devices [9], [10]. Conventional models based on polynomial or logarithmic basis fail to fit the signals with high accuracy due to their non-monotonic, under-sampled nature, continuously varying slopes due to damping factors, presence of noise and higher-order perturbation in the signals [11]. While recently developed fitting techniques, such as Gaussian process regression and machine learning techniques can provide a high accuracy fit, these are data-based techniques and thus provide no information and understanding about the device physics [12]–[14].

Prony's method is a parametric method to fit a sum of damped complex exponentials to the measurement data [15]–[17]. Prony's method is a powerful signal processing and system identification technique as it offers the advantages of identifying damping coefficients apart from frequency, phase, and amplitude and is thus superior to Fourier analysis [18]. While Prony's method was invented by Gaspard de Prony in 1795 to solve a recovery problem in physical chemistry [19], the strengths of this technique have been lately exploited in several applications over the past few decades including radar signal processing, super-resolution, signal deconvolution, parameter estimation, filter design and electrical power system electromechanical modes identification [20]–[24].

In this work, we propose a Prony-based curve-fitting method to characterize RF pulse measurements from optoelectronic devices. The measurements are obtained from a novel photoconductive semiconductor switch device that operates as a high frequency, high power RF source or amplifier [25]. Based on the semiconductor physics of optoelectronic devices, the RF pulse output of such devices has a rising half, which is a function of the input Gaussian pulse, and a decaying half that is representative of exponential time constants of the carrier lifetime in the semiconductor. Thus, a Gaussian fitting approach is used to fit the rising half of the signal followed by a Prony fitting approach to fit the decaying fall of the signal [11], [26]. Key RF parameters, such as full width at half maximum (FWHM), bandwidth, rise time, fall time and gain of the measured signals

Manuscript received October 27, 2021; revised November 30, 2021; accepted November 30, 2021. Date of publication December 15, 2021; date of current version January 28, 2022. This work was supported in part by the U.S. Department of Energy by Lawrence Livermore National Laboratory under Grant DE-AC52-07NA27344, in part by the LLNL-LDRD Program under Grant 19-DR-015, and in part by the Lawrence Livermore National Laboratory Contribution under Grant LLNL-JRNL-LLNL-826272. The associate editor coordinating the review of this manuscript and approving it for publication was Dr. Lu Gan. *(Corresponding author: Saptarshi Mukherjee.)*

Saptarshi Mukherjee, Karen Dowling, and Lars Voss are with the Lawrence Livermore National Laboratory, Livermore, CA 94550 USA (e-mail: mukherjee5@llnl.gov; dowling7@llnl.gov; voss5@llnl.gov).

Yicong Dong, Kexin Li, and Shaloo Rakheja are with the University of Illinois at Urbana-Champaign, Champaign, IL 61820 USA (e-mail: yicongd2@illinois.edu; kexinli4@illinois.edu; rakheja@illinois.edu).

Adam Conway is with Raytheon Technologies, Waltham, MA 02451 USA (e-mail: conway8@llnl.gov).

This letter has supplementary downloadable material available at https://doi.org/10.1109/LSP.2021.3135795, provided by the authors.

Digital Object Identifier 10.1109/LSP.2021.3135795

Algorithm 1: Prony fitting method.

Input: Measured data: $y_{\text{meas}}(t)$
Output: Fitted curve: $y_{\text{fit}}(t)$, Prony time constants (τ)
1: Create a $k \times k$ Hankel matrix H from $y_{\text{meas}}(t)$
2: Find Prony order (p) from eigen value distribution of H
3: Form polynomial matrix X from Z-transform of (3)
4: Find α_k in the time domain by obtaining roots of matrices derived from $Z(y_{\text{trap}})$ and X [1]
5: Find amplitudes c_k from inverse Z-transform operations.

can be extracted from the fitted curves and used to characterize the performance of the devices. Additionally the capability of the method to extract multiple time constants due to long tails associated with semiconductor traps can help in better understanding of the device physics [27]. The overall efficiency of the method is demonstrated by obtaining high accuracy fitting of varied waveform shapes. The effect of the system order on the fitting accuracy, as well as the robustness of the proposed fitting technique towards measurement noise, sampling rate and repeatability is demonstrated.

The key novelty of this approach over existing curve-fitting techniques is the development of an algorithm that can directly compute the system order to determine how many dominant traps are present in the semiconductor and then optimize the material growth and device fabrication to optimize those dominant traps. Unlike different non-linear, iterative least squares-based curve-fitting approaches that are computationally intensive and are complicated to implement, the proposed algorithm is non-iterative and easy to implement [28]. Further, the algorithm shows its capability to accurately characterize under-sampled RF signals corresponding to the optoelectronic devices. The algorithm is fully automated to analyze large volumes of data for extensive device testing and optimization over a broad design space. Finally, the algorithm is fine-tuned to handle the complexities of RF pulse measurements from optoelectronic devices such as long decaying tail, pulse distortion, non-monotonicity, measurement noise and under-sampling.

II. Prony-Based Algorithm

An RF pulse $y_{\text{meas}}(t)$ generated by [1]the photoconductive switch [25] consists of a rising main peak followed by a slowly decaying fall [29], [30]. The overall curve-fitting algorithm to extract the fitted curve $y_{\text{fit}}(t)$ can be divided into two primary steps, 1: fitting the rise of the signal ($y_{\text{main}}(t)$) and 2: fitting the fall of the signal ($y_{\text{trap}}(t)$). The overall objective of the algorithm is to minimize the root mean square error ϵ between $y_{\text{meas}}(t)$ and $y_{\text{fit}}(t)$ normalized by the peak voltage (v_p) of $y_{\text{meas}}(t)$ and expressed as a percentage. It is given by

$$\epsilon = \frac{\sqrt{\left(\sum_{i=1}^{i=n} \left(y_{\text{fit}}(i) - y_{\text{meas}}(i)\right)/n\right)^2}}{v_p}, \tag{1}$$

[1]Roots can be real α_k as well as complex $\alpha_k + j\omega_k$.

where $y_{\text{fit}} = y_{\text{main}} + y_{\text{trap}}$ and n is the number of time steps.

A. Gaussian Fitting

$y_{\text{main}}(t)$ is computed using a Gaussian distribution function expressed as

$$y_{\text{main}}(t) = Ae^{-\frac{(t-t_p)^2}{2\sigma^2}}, \quad \text{where } 0 < t \leq t_p, \tag{2}$$

where A is the peak value of the signal, t_p is the time instant at the signal peak, and σ^2 is the calculated variance of the Gaussian distribution function.

B. Prony Fitting

Prony's method is utilized to fit a sum of damped complex exponentials to $y_{\text{trap}}(t)$ expressed as [31]

$$y_{\text{trap}}(t) = \sum_{k=1}^{p} c_k z_k^n, \quad \text{where } t_p < t \leq t_n, \tag{3}$$

where $z_k = e^{-\alpha_k}$.The three unknowns that need to be computed are the k_{th} damping coefficient α_k, the amplitude of k_{th} component c_k, and the order of the prony fit p. The mathematical foundations of the Prony method have been discussed in details in [20], [32]. For the sake of brevity, we skip the mathematical equations and outline the steps in an algorithmic framework (Algorithm 1) [33].

Fig. 1 shows the implementation of the Prony-based algorithm on a measured RF pulse signal. A typical transient RF waveform measured by the photoconductive semiconductor switch device, subjected to an input pulse waveform [25], is shown in Fig. 1(a). As mentioned before, the rising signal is fitted using a Gaussian distribution function (Fig. 1(b)), while the decaying tail signal is fitted using the Prony's method (Fig. 1(c)) [27]. The order of the Prony fit (p) is computed based on Step 2 of Algorithm 1 and was chosen to be 3, as shown in the inset of Fig. 1(c). The final fitted curve $y_{\text{fit}}(t)$ is closely matched with $y_{\text{meas}}(t)$. Some of the higher-order data fluctuations in the signal tail are not captured in $y_{\text{fit}}(t)$ due to the lower-order of the Prony fit.

III. Effect of Order of Prony Fit

In this section, we study the effect of Prony order on the fitting accuracy. The order of the Prony series (p) can be found out from its eigen value decomposition, given by $\text{eigen}(H) \approx 0$. It is important to note that the calculation of p does not require plotting the eigen values of H, but based on an automated error criterion, given by [20]

$$\text{eigen}(H) \leq \delta, \tag{4}$$

where δ is chosen such that λ_k decays to 0.1% (30 dB) of its highest eigen value. The automated calculation of p helps determine how many dominant traps are present in the semiconductor and their frequency response, which can be used to optimize the material growth and device fabrication to optimize those dominant traps.

The above principal is tested using a pulsed measurement of a fabricated optoelectronic device. The waveform is a broad, non-monotonic pulse (FWHM$\sim$2 ns) with significant distortion

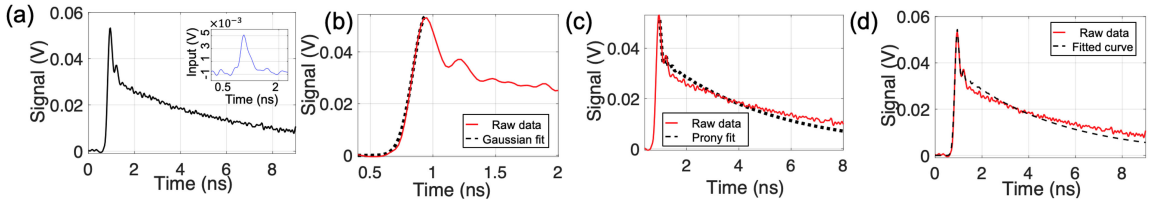

Fig. 1. Overall approach of the curve-fitting method: (a) RF pulse measured $y_{\text{meas}}(t)$ by an optoelectronic device showing the rising main peak followed by a slowly decaying fall with long tail, the input laser pulse fed to the device is shown in the inset. (b) Fitting the rise of the signal ($y_{\text{main}}(t)$) using a Gausian distribution function. (c) Fitting the fall of the signal ($y_{\text{trap}}(t)$) using Prony fitting, (d) Overall fitting performance of $y_{\text{fit}}(t) = y_{\text{main}}(t) + y_{\text{trap}}(t)$.

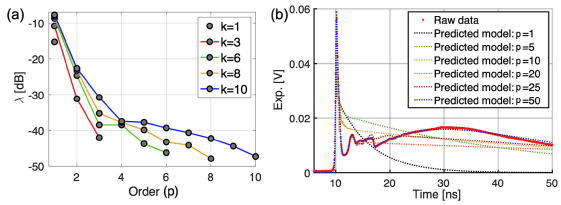

Fig. 2. Effect of order of Prony series on the fitting accuracy of a measured waveform: (a) Plot of the eigen values λ if the Hankel matrix vs k for various sizes of H matrix, p can be determined from the condition stated in (4), (b) Fitting results show that the major exponential decay can be captured by low-order Prony series, higher-order fluctuations and non-monotonic oscillatory trends in the measured data are captured by higher-order of Prony series.

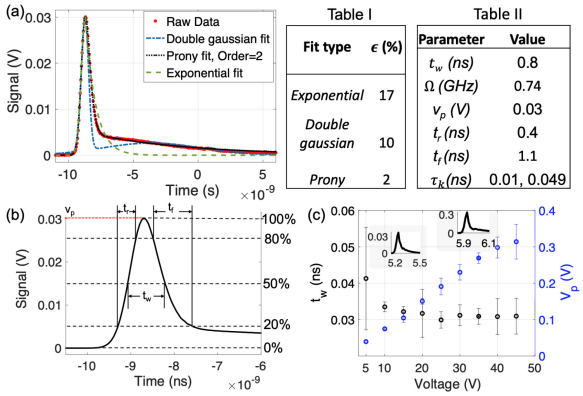

Table I

Fit type	ϵ (%)
Exponential	17
Double gaussian	10
Prony	2

Table II

Parameter	Value
t_w (ns)	0.8
Ω (GHz)	0.74
v_p (V)	0.03
t_r (ns)	0.4
t_f (ns)	1.1
τ_k (ns)	0.01, 0.049

Fig. 3. Performance of the fitting method: (a) Comparison of fitting accuracy between a conventional double Gaussian fitting method and the proposed Prony method, (b) RF pulse and its parameters (t_w, v_p, t_r, t_f), (c) Key RF performance metrics FWHM (t_w) and peak voltage (v_p) obtained from the Prony fitting technique. Table I shows a comparison of the fitting error, ϵ, between the two fitting methods in Fig. 3(a). Higher accuracy of the proposed method is demonstrated. Table II shows the extracted RF performance metrics obtained from the fitting results of the measured data plotted in Fig. 3(a).

in the tail in the form of high-order oscillations along with a slow, second peak as shown in Fig. 2(b). The eigen value plot in Fig. 2(a) show smaller drop of λ with increasing order from $p = 3$ to $p = 10$. The results of Prony fitting show that while the Prony fit with lower-orders ($p = 1, 5$) captures part of the major exponential decay, higher-order Prony fits ($p = 10, 20$) are not captured. However, higher-order Prony fits ($p = 25, 50$) can capture the non-monotonic oscillatory trends, as well as the second peak. This result demonstrates the robustness of the curve-fitting method towards different types of optoelectronic signals with varying pulse dynamics such as pulse width variation and higher-order distortions.

IV. Characterization of RF Pulses

Fig. 3(a) shows a comparison of fitting accuracy of an RF pulse measurement between Prony and two different techniques. Since the laser input is a Gaussian pulse while the output pulse has a decaying tail, both Gaussian and exponential fitting techniques are considered. Fig. 3(a) shows that while the rising pulse is well characterized by all three techniques, the decaying tail is not accurately fitted with a double Gaussian fitting due to the slope associated with the unique shape of the waveform, and also not accurately fitted with a single exponential fitting due to higher-order perturbation in the signals. On the other hand, a second-order Prony series provides a more accurate fit, with an 8% improvement in error over the other techniques (Table I). While techniques such as Gaussian process regression can provide high accuracy fit, these are data-based techniques and thus do not correlate the extracted fitting parameters with the underlying device physics.

After an accurate fitting is achieved, key RF parameters such as pulse width (t_w), bandwidth (Ω), rise time (t_r), fall time (t_f) and v_p of the measured signals are extracted from the fitted curves. t_w is expressed as the FWHM of the pulse, t_r is measured as the time delay for a signal to move from 20% of v_p to 80% of v_p during the rise of the signal, t_f is measured as the time delay for the signal to move from 80% of v_p to 20% of v_p during the fall of the signal. These parameters are shown in Fig. 3(b). Ω is expressed as $1/t_w$ [34]. The RF parameters obtained for the measured waveform in Fig. 3(a) is shown in Table II and correlate well with prior experiments and simulations, thus verifying the reliability of the approach [25], [35]. The algorithm has been automated to analyze large volumes of data in order to analyze the effect of different experimental parameters on the device's performance. As an example, the effect of increasing the strength of electric field on the device was studied using the algorithm. t_w and v_p were extracted after performing fitting analysis from 50 experimental measurements, and plotted in Fig. 3(c). The analysis shows the correlation between t_w, v_p and the applied electrical voltage, as well as the variability in the measured parameters, represented by the error bars. This information can be used to optimize experimental settings as

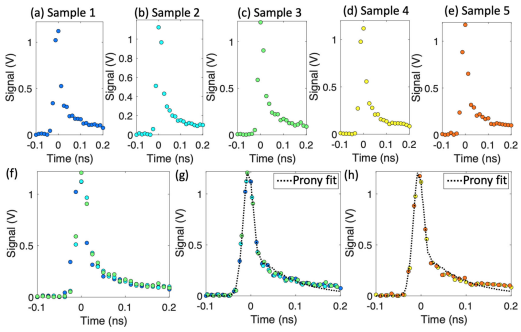

Fig. 4. (a)–(e) 5 repeated under-sampled measurements corresponding to the same device, (f) Raw data from the first 3 measurements (Samples 1,2, 3) plotted on top of each other showing that there needs to be time shifting to properly align the data, (g) Aligned data waveform after time-shifting and its corresponding Prony fitting model, (h) Fitting accuracy of the Prony fitting model for the remaining 2 measurements (Samples 4, 5).

well as the design of the device to achieve the device's ideal performance.

V. Semiconductor Physics From Prony Constants

The Prony time constants (τ from Table II) extracted for the photoconductivity measurements of an optoelectronic device reported here are representative of the carrier lifetime in the semiconductor. The zeroth-order mode of Prony series, corresponding to the largest time constant in the system (say τ_1), contains both bulk and surface contributions [36]. That is,

$$\tau_1^{-1} = \tau_{\text{bulk}}^{-1} + b_1 \mathcal{D}, \tag{5}$$

where τ_{bulk} is the bulk lifetime, b_1 is a constant (related to the amplitude of the mode), and $\mathcal{D}$ is the carrier diffusivity. For samples with dominant surface recombination, the surface recombination velocity of carriers can be determined by measuring the lifetimes of two samples with different thicknesses and similar surface treatment.

The Prony time constants can also be used to interpret the defect properties, i.e., the activation energy and cross-section of the defect, in the semiconductor. The Prony method can be used to extract the time constants from measurements at various temperatures to reveal defect-specific information [12], [13]. For electrons, the defect properties are found using [37]

$$\tau_t T^2 = \frac{\exp \frac{E_a}{k_B T}}{\sigma_t \gamma}, \tag{6}$$

where τ_t is a Prony time constant, T is the sample temperature, E_a is the activation energy of the defect state, σ_t is the electron capture cross-section, and γ is a material-specific constant. An Arrhenius plot of the emission process (i.e., $\ln(T^2 \times \tau_t)$ versus $1/k_B T$) provides information on the activation energy of the trap, $(E_c - E_t)$, and σ_t.

VI. Repeatability and Under-Sampling

In this section, we demonstrate the robustness of the Prony fitting technique towards noise, sampling rate and repeatability. Figs. 4(a)–(e) shows five repeated under-sampled measurements corresponding to an optoelectronic device [25]. We use the first three measurements to create a well-sampled data and generate the Prony fitting model. This model is then used to test the fitting accuracy for the remaining two measurements.

The lack of data points covering the rise and fall of the signal lead to under-sampled waveforms due to the sampling limits imposed by Nyquist criterion. While the individual raw data waveforms are under-sampled, with five points covering the rise and fall of the signal, the waveforms can be combined to have more data points representing the signal, thus reducing under-sampling. Due to time delays associated with each measurement, the waveforms do not properly align, as seen from the raw data from the first three measurements (Samples 1,2,3) plotted on top of each other (Fig. 4(f)). With respect to a reference measurement, the time delays for the remaining measurements are manually calculated and a "time shifting" approach is applied to align the signals as follows: $g_n(t) = f_n(t + e_n)$, where $f_n(t)$ is the raw waveform, $g_n(t)$ is the time-shifted waveform, e_n is the time shift and n is the corresponding measurement. After performing time-shifting, the final data waveform shows perfect time-alignment, with its corresponding Prony fit model accurately fitting the waveform (Fig. 4(g)). While the example shows manual alignment, this process will be automated using a least-squares-based correlation technique as part of future work [38].

The remaining two measurements (Samples 4, 5) are plotted on top of the Prony fit model in Fig. 4(h) and shows highly accurate fitting of the data points especially along the rise and fall of the signal. This demonstrates the anti-noise and repeatable calculation properties of the Prony algorithm. It is critical to mention that the additional higher-order fluctuations due to measurement noise along the fall of the signal is intentionally not fitted using higher Prony order, so that the approach does not fit the noise component of the signal and reduce overfitting. Some additional strengths and limitations of the approach are shown in a supplementary figure.

VII. Conclusion

A Prony-based curve-fitting technique is developed to characterize RF pulse measurements from optoelectronic devices. The algorithm is described and demonstrated with fitting of different experimental waveforms. While lower-order Prony fitting captures the major exponential decay, fluctuations along the decaying tail are progressively captured by higher-order fitting. Based on the experimental datasets analyzed, the proposed approach performs better than other curve-fitting techniques with an 8% improvement in error. The approach extracts the time constants associated with semiconductor traps that provides understanding about the device physics that other curve-fitting techniques do not capture. The robustness of the fitting technique towards noise, sampling rate and repeatability associated with experimental measurements are discussed discussed to provide a holistic understanding about its performance. Future work will be focused on automated processing of repeated measurements to accurately fit under-sampled signals. Additionally, upgrades to the algorithm to deal with higher-order oscillations in the signal tail will be investigated [39], [40]. Finally, while the current technique can only process uniformly sampled data, techniques to process non-uniformly sampled data will be developed [41].

REFERENCES

[1] J. Allam, "Semiconductor optoelectronic devices," *High Press. Semicond. Phys. II*, p. 301, 1998.

[2] X. Wang, Y. Cui, T. Li, M. Lei, J. Li, and Z. Wei, "Recent advances in the functional 2D photonic and optoelectronic devices," *Adv. Opt. Mater.*, vol. 7, no. 3, 2019, Art. no. 1801274.

[3] M. Bora *et al.*, "A total internal reflection photoconductive switch," *IEEE Electron Device Lett.*, vol. 40, no. 5, pp. 734–737, May 2019.

[4] A. Conway, S. E. Harrison, R. J. Nikolic, Q. Shao, and L. Voss, "Three dimensional vertically structured electronic devices," US Patent 11,024,734, Jun. 01 2021.

[5] J. Liao, J. Zeng, S. Deng, A. O. Boryssenko, V. M. Joyner, and Z. R. Huang, "Packaging of dual-mode wireless communication module using RF/optoelectronic devices with shared functional components," *IEEE Trans. Adv. Packag.*, vol. 33, no. 2, pp. 323–332, May 2010.

[6] J. G. McCall *et al.*, "Fabrication and application of flexible, multimodal light-emitting devices for wireless optogenetics," *Nature Protoc.*, vol. 8, no. 12, pp. 2413–2428, 2013.

[7] T. Hao *et al.*, "Recent advances in optoelectronic oscillators," *Adv. Photon.*, vol. 2, no. 4, 2020, Art. no. 44001.

[8] M. Razeghi, "III-Nitride optoelectronic devices: From ultraviolet toward terahertz," *IEEE Photon. J.*, vol. 3, no. 2, pp. 263–267, Apr. 2011.

[9] T. S. Wolfe *et al.*, "Integrated computational investigation of photoconductive semiconductor switches in pulsed power radio frequency applications," *IEEE Plasma Sci.*, vol. 44, no. 1, pp. 60–70, 2015.

[10] R. C. Qiu, C. Zhou, and Q. Liu, "Physics-based pulse distortion for ultra-wideband signals," *IEEE Trans. Veh. Technol.*, vol. 54, no. 5, pp. 1546–1555, Sep. 2006.

[11] S. Rakheja, K. Li, K. M. Dowling, A. M. Conway, and L. F. Voss, "Design and simulation of near-terahertz GaN photoconductive switches-operation in the negative differential mobility regime and pulse compression," *IEEE J. Electron Devices Soc.*, vol. 9, pp. 521–532, May 2021.

[12] J. Q. Shi and B. Wang, "Curve prediction and clustering with mixtures of Gaussian process functional regression models," *Statist. Comput.*, vol. 18, no. 3, pp. 267–283, 2008.

[13] Z. Jiang, D. Zhang, and G. Lu, "Radial artery pulse waveform analysis based on curve fitting using discrete Fourier series," *Comput. Methods Programs Biomed.*, vol. 174, pp. 25–31, 2019.

[14] P. Vidyullatha and D. R. Rao, "Machine learning techniques on multidimensional curve fitting data based on R-square and chi-square methods," *Int. J. Elect. Comput. Eng.*, vol. 6, no. 3, pp. 974–979, 2016.

[15] J. J. Sacchini, W. M. Steedly, and R. L. Moses, "Two-dimensional Prony modeling and parameter estimation," *IEEE Trans. Signal Process.*, vol. 41, no. 11, pp. 3127–3137, Nov. 1993.

[16] D. Potts and M. Tasche, "Parameter estimation for exponential sums by approximate Prony method," *Signal Process.*, vol. 90, no. 5, pp. 1631–1642, 2010.

[17] T. Peter and G. Plonka, "A generalized prony method for reconstruction of sparse sums of eigenfunctions of linear operators," *Inverse Problems*, vol. 29, no. 2, 2013, Art. no. 025001.

[18] S. U. Pillai and H. S. Oh, "Resonant mode extraction from scattered noisy data," in *Proc. IEEE 28th Asilomar Conf. Signals Syst. Comput.*, 1994, pp. 816–820.

[19] R. Prony, "Essai experimental et analytique: sur les lois de la dilatabilite des fluides elastique et sur celles de la force expansive de la vapeur de l'eau et de la vapeur de l'alkool, a differentes temperatures," *J. de l'cole Polytechnique*, vol. 2, 1795.

[20] R. Carriere and R. L. Moses, "High resolution radar target modeling using a modified Prony estimator," *IEEE Trans. Antennas Propag.*, vol. 40, no. 1, pp. 13–18, Jan. 1992.

[21] P. Wang and X. Li, "Hybrid sparse expansion and separable hybrid Prony method," *IEEE Trans. Signal Process.*, vol. 69, pp. 3033–3043, May 2021.

[22] A. E. Siegman and H. Miller, "Unstable optical resonator loss calculations using the Prony method," *Appl. Opt.*, vol. 9, no. 12, pp. 2729–2736, 1970.

[23] M. Tawfik and M. Morcos, "ANN-based techniques for estimating fault location on transmission lines using Prony method," *IEEE Trans. Power Del.*, vol. 16, no. 2, pp. 219–224, Apr. 2001.

[24] C. W. Therrien and C. H. Velasco, "An iterative Prony method for Arma signal modeling," *IEEE Trans. Signal Process.*, vol. 43, no. 1, pp. 358–361, Jan. 1995.

[25] K. Dowling *et al.*, "Compression photoconductive switching using negative differential mobility," *IEEE Trans. Electron. Devices*, early access, Dec. 2021, doi: 10.1109/TED.2021.3136500

[26] L. F. Voss and A. M. Conway, "Tunnel drift step recovery diode," U.S. Patent App. 17/081,902, Apr. 29 2021.

[27] J. Joh and J. A. Del Alamo, "A current-transient methodology for trap analysis for GaN high electron mobility transistors," *IEEE Trans. Electron Devices*, vol. 58, no. 1, pp. 132–140, Jan. 2011.

[28] N. Chernov, C. Lesort, and N. Simányi, "On the complexity of curve fitting algorithms," *J. Complexity*, vol. 20, no. 4, pp. 484–492, 2004.

[29] A. Abur and H. Singh, "Time domain modeling of external systems for electromagnetic transients programs," *IEEE Trans. Power Syst.*, vol. 8, no. 2, pp. 671–679, May 1993.

[30] J.-H. Hong and J.-K. Park, "A time-domain approach to transmission network equivalents via Prony analysis for electromagnetic transients analysis," *IEEE Trans. Power Syst.*, vol. 10, no. 4, pp. 1789–1797, Nov. 1995.

[31] T. Sauer, "Prony's method: An old trick for new problems," Mathematisches Forschungsinstitut Oberwolfach, 2018.

[32] V. Slyusar, "Interpretation of the Proni method for solving long-range problems," *Radio Electron. Commun. Syst. Izvestiia-Vysshie Uchebnye*, vol. 41, pp. 35–39, 1998.

[33] T. Sauer, "Prony's method in several variables," *Numer. Math.*, vol. 136, no. 2, pp. 411–438, 2017.

[34] M. Ghavami, L. Michael, and R. Kohno, *Ultra Wideband Signals and Systems in Communication Engineering*. Hoboken, NJ, USA: Wiley, 2007.

[35] S. Rakheja, L. Huang, S. Hau-Riege, S. Harrison, L. F. Voss, and A. M. Conway, "Performance modeling of silicon carbide photoconductive switches for high-power and high-frequency applications," *IEEE J. Electron Devices Soc.*, vol. 8, pp. 1118–1128, Sep. 2020.

[36] S. S. Li, *Semiconductor Physical Electronics*. Berlin, Germany: Springer, 2012.

[37] A. R. Arehart, "Investigation of electrically active defects in GaN, AlGaN, and AlGaN/GaN high electron mobility transistors," Ph.D. dissertation, Ohio State Univ., Columbus, OH 43210, USA, 2009.

[38] E. W. Weisstein, "Least squares fitting," Aug. 29, 2002. [Online]. Available: https://mathworld.wolfram.com/

[39] A. M. Groopman *et al.*, "Conventional, Bayesian, and modified Prony's methods for characterizing fast and slow waves in equine cancellous bone," *J. Acoust. Soc. Amer.*, vol. 138, no. 2, pp. 594–604, 2015.

[40] J. Murray-Bruce and P. L. Dragotti, "A sampling framework for solving physics-driven inverse source problems," *IEEE Trans. Signal Process.*, vol. 65, no. 24, pp. 6365–6380, Dec. 2017.

[41] L. Coluccio, A. Eisinberg, and G. Fedele, "A Prony-like method for non-uniform sampling," *Signal Process.*, vol. 87, no. 10, pp. 2484–2490, 2007.